

## Article

# Transmission Characteristics and Spatial Coherence of Partially Coherent Light-Emitting Diode Array in the Ocean

Zhifang Miao <sup>1</sup>, Xiang'e Han <sup>2,\*</sup>, Qiyu Wang <sup>2</sup>, Fang Lu <sup>2</sup> and Qiwei Li <sup>2</sup>

<sup>1</sup> School of Telecommunication Engineering, Xidian University, Xi'an 710071, China; zfmiaoxidian@foxmail.com

<sup>2</sup> School of Physics, Xidian University, Xi'an 710071, China; awangwang304@163.com (Q.W.); lufang11@163.com (F.L.); lqw17@xidian.edu.cn (Q.L.)

\* Correspondence: xehan@mail.xidian.edu.cn

**Abstract:** Underwater LED light sources are commonly implemented in array configurations with a wide-angle field of view, primarily catering to high-speed communication within a few meters. To increase transmission distance and mitigate oceanic turbulence effects, this paper focuses on the spatial coherence analysis of narrow-beam partially coherent light-emitting diode (PCLED) arrays, examining their average light intensity distribution, beam width, and spatial coherence during oceanic transmission. Based on the extended Huygens–Fresnel integral, the optical field models and spatial characteristics of the radial PCLED array are derived under oceanic conditions, considering parameters such as water attenuation coefficient, kinetic energy dissipation rate, temperature dissipation rate, temperature-to-salinity ratio, as well as the radial filling factor and the sub-beam spatial coherence length of the light source at different transmission distances. The simulations show that, as the spatial coherence length of the sub-beam decreases from hundreds to a few micrometers, the combining distance of the beam arrays also decreases. This reduction in coherence results in the average light intensity distribution degrading into a Gaussian-like distribution, with a significant five-fold decrease in peak intensity. Furthermore, the width of the array spreads, starting from distances of 7 m and 0 m, respectively. The radial PCLED beam array, with its sub-beam spatial coherence length inside micrometers, possesses inherent characteristics that suppress turbulence effects and has future extensive possibilities in the ocean.

**Keywords:** light-emitting diode; oceanic turbulence; attenuation; extended Huygens–Fresnel; array beam spreading



**Citation:** Miao, Z.; Han, X.; Wang, Q.; Lu, F.; Li, Q. Transmission Characteristics and Spatial Coherence of Partially Coherent Light-Emitting Diode Array in the Ocean. *Photonics* **2023**, *10*, 1049. <https://doi.org/10.3390/photonics10091049>

Received: 1 August 2023

Revised: 1 September 2023

Accepted: 8 September 2023

Published: 15 September 2023



**Copyright:** © 2023 by the authors. Licensee MDPI, Basel, Switzerland. This article is an open access article distributed under the terms and conditions of the Creative Commons Attribution (CC BY) license (<https://creativecommons.org/licenses/by/4.0/>).

## 1. Introduction

With the increasing demand for real-time transmission of images and videos from unmanned equipment in underwater optical communication, there is a growing need to enhance the quality of optical communication and extend the transmission distance [1,2]. Beamforming has emerged as an effective technique. However, the performance of laser arrays used in ocean environments is adversely affected by oceanic turbulence, resulting in phase distortions, beam divergence, and displacement. To tackle these challenges, researchers have found that altering beam coherence could mitigate turbulence effects. Based on the extended Huygens–Fresnel integral and the power spectrum of oceanic turbulence [3], this research area has garnered significant attention from the academic community, leading to diverse achievements, including studies on partially coherent laser beams [4–6] and array beams [7–9], among other notable studies.

The light-emitting diode (LED) offers a range of advantages, including low cost, high reliability and stability, ease of integration, and controllability. These arrays are commonly described as the amalgamation of fully incoherent beams using the Lambertian model [6], surpassing laser arrays with partially coherent beams in the presence of oceanic turbulence

effects [10]. The spatial coherence of the beam significantly influences various aspects, including the sensitivity of the optical detection system, requirements for detector size, information transmission capacity, and resistance to interference, rendering it an indispensable consideration. Currently, in the modeling and simulation process of light beams, the spatial coherence lengths of partially coherent laser beams and LEDs are typically considered to range from infinity to millimeters and micrometers, respectively [11–13]. Some high-power LEDs or specially designed LEDs modulated by the coherence structure can potentially mitigate the negative effect of the channel [14–16]. Unlike existing studies on fully incoherent light from LEDs and partially coherent light from laser arrays with large spatial coherence lengths, further exploration and analysis are needed for partially coherent light LED arrays at the micrometer scale, considering the significant variations in average light intensity distribution, beam spreading, and spatial coherence.

In this paper, we extend our research beyond the analysis of the combined effects of channel attenuation and oceanic turbulence. Building upon previous work [17], we also consider the partial coherence of the LED array. It is essential to incorporate the variations in optical intensity attenuation, beam spreading, and coherence during the optical transmission. These variations significantly impact optical detection, channel capacity, and the signal-to-noise ratio of oceanic systems. By comprehensively understanding these effects and implementing suitable signal processing, we can enhance the performance and reliability of underwater systems while further advancing the development and application of underwater optical communication technology.

## 2. Propagation Theory

### 2.1. PCLED Beam Array Model

The LED beam can utilize two mathematical models, namely the Lambertian model and the Gaussian model, to describe its light field distribution [10]. The narrow beam light field  $E(\mathbf{r}, z_1, t)$  satisfies the Gaussian distribution property under the conditional constraints of  $\Phi_{1/2} \leq 10^\circ$ ,  $r^2 \ll z_1^2$ , where  $\Phi_{1/2}$  is the half-power angle and  $z_1$  refers to the distance from the LED light emission area. The expression for the complex amplitude on the observation plane at  $z = z_1$  is given by [17].

$$U(\mathbf{r}, z_1, t) = |E(\mathbf{r}, z_1, t)|^{1/2} \exp\{-i\phi(\mathbf{r}, t)\} = \left(\frac{(m+1)E_0}{2\pi z_1^2}\right)^{1/2} \exp\left\{-\frac{r^2}{w^2(z_1)}\right\} \exp\{-i\phi(\mathbf{r}, t)\} \quad (1)$$

where  $\mathbf{r}(x, y)$  is the position vector on the  $z_1$ -plane,  $E_0$  is the center radiation illuminance of the light source,  $m$  is the Lambertian order, and  $m = -\ln(2)/\ln(\cos(\Phi_{1/2}))$ . The smaller the half-power angle of  $\Phi_{1/2}$  is, the larger the value of  $m$  is, and the narrower the range of the LED radiation angle is, and the  $\phi(\mathbf{r}, t)$  meets  $(-\pi, \pi)$  on the random phase.

Unlike incoherent sources like thermal light sources (such as incandescent bulbs), LEDs have a more ordered emission process due to the confinement of light within a small semiconductor region. If the LED light radiation satisfies Equation (1), the spatial coherence distribution also satisfies the Gaussian function [18]. Let  $P_0 = \left(\frac{(m+1)E_0}{2\pi z_1^2}\right)$  and  $\sigma_0$  be the amplitude and the spatial coherence length of the  $z_1$ -plane light field, respectively.  $\mathbf{s}_1 = (s_{1x}, s_{1y})$ ,  $\mathbf{s}_2 = (s_{2x}, s_{2y})$  denote an arbitrary point in the plane of  $z = z_1$ , and  $w_0 = w(z_1)$  represents the waist diameter. In order to describe the derivation process of the optical transmission more clearly, we take the  $z_1$ -plane as the initial surface of the system, i.e.,  $L = 0$ , and analyze the transmission characteristics. At this moment, the description of the LED with partial coherence can be abbreviated as PCLEDs (partially coherent light-emitting diodes, PCLEDs). Following the spatial coherence characteristics of partially coherent optical transmission theories, from Equation (1) the cross-spectral density function (CSDF) expression of narrow-beam LED is given as

$$W(\mathbf{s}_1, \mathbf{s}_2, 0) = P_0 \exp\left\{-\frac{(\mathbf{s}_1^2 + \mathbf{s}_2^2)}{w_0^2}\right\} \exp\left[-\frac{(\mathbf{s}_1 - \mathbf{s}_2)^2}{2\sigma_0^2}\right] \quad (2)$$

The following will consider the LED array light field consisting of satisfying Equation (2) as depicted in Figure 1. Assuming there are  $N = 8$  identical LED beams distributed uniformly on a circular ring of radius  $r_0$  in the Cartesian coordinate system, the angular spacing between adjacent sub-beams is denoted as  $\alpha_0 = 2\pi/N$ . The angle between any beam located on the ring and the  $x$ -axis can be represented as  $\alpha_n = n\alpha_0$  ( $n = 0, 1, 2, \dots, N - 1$ ). The other parameters are shown in Table 1.

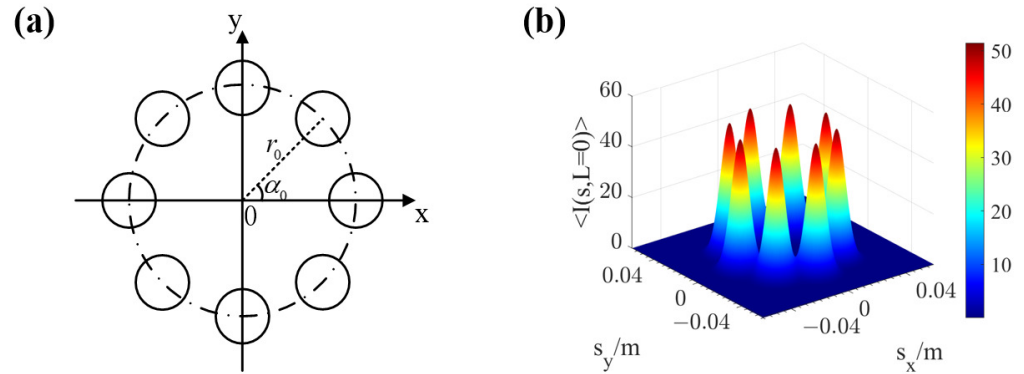


**Figure 1.** Schematic diagram of radial LED beam array ( $L = 0$ ): (a) 2D array layout and (b) 3D array layout.

Taking into account the partial coherence of LEDs and in combination with Equation (2), the expressions for the CSDF at the  $L = 0$  plane for the PCLED arrays can be obtained, which are composed of individual sub-beams. The CSDF can be described as follows, by the method of coherent synthesis [19]:

$$W^{(0)}(\mathbf{s}_1, \mathbf{s}_2, 0) = \sum_{n=1}^N \sum_{m=1}^N P_n \exp \left[ -\frac{(\mathbf{s}_1 - \mathbf{r}_n)^2 + (\mathbf{s}_2 - \mathbf{r}_m)^2}{w_0^2} \right] \exp \left[ -\frac{[(\mathbf{s}_1 - \mathbf{r}_n) - (\mathbf{s}_2 - \mathbf{r}_m)]^2}{2\sigma_0^2} \right] \quad (3)$$

where  $P_n = NP_0$  represents the initial array optical amplitude.  $\mathbf{r}_n = (r_0 \cos \alpha_n, r_0 \sin \alpha_n)$  represents the center of the  $n$ th PCLED beam.

### 2.2. Transmission Characteristics of PCLED Array Beams in the Ocean

The transmission of various array beams in ocean is subject to the influences of absorption, scattering, and turbulence effects. The mathematical description of the effect of absorption and scattering by seawater on the average light intensity from  $(\mathbf{s}, 0)$  to  $(\boldsymbol{\rho}, L)$  is given by [20]:

$$\langle I_{att}(\boldsymbol{\rho}, L) \rangle = \langle I_0(\mathbf{s}, 0) \rangle e^{-(a+b)L} \quad (4)$$

where  $\langle I_0(\mathbf{s}, 0) \rangle$  and  $\langle I_{att}(\boldsymbol{\rho}, L) \rangle$  is the average light intensity of the initial array and observing plane, respectively.  $a$  and  $b$  are the absorption and scattering attenuation coefficients of the water, respectively, which vary with different parameters such as temperature, salinity, and light wavelength. Let  $c = a + b$  represent the combined attenuation effect. The comprehensive literature [21] and experimental measurement and specific typical attenuation parameters are shown in the simulation.

Under the assumption of paraxial transmission conditions in a homogeneous isotropic oceanic turbulent medium, the CSDF of the beam in turbulence at a transmission distance of  $L$ , as described by the extended Huygens–Fresnel integral, can be expressed as [5]

$$W(\boldsymbol{\rho}_1, \boldsymbol{\rho}_2, L) = \left( \frac{k}{2\pi L} \right)^2 \iiint \iiint d^2\mathbf{s}_1 d^2\mathbf{s}_2 W^{(0)}(\mathbf{s}_1, \mathbf{s}_2, 0) \times \exp \left[ ik \frac{(\boldsymbol{\rho}_1 - \mathbf{s}_1)^2 - (\boldsymbol{\rho}_2 - \mathbf{s}_2)^2}{2L} \right] \times \langle \exp[\psi(\mathbf{s}_1, \boldsymbol{\rho}_1, L) + \psi^*(\mathbf{s}_2, \boldsymbol{\rho}_2, L)] \rangle \quad (5)$$

where  $\rho_1 = (\rho_{1x}, \rho_{1y})$  and  $\rho_2 = (\rho_{2x}, \rho_{2y})$  represent any two points in the receiving plane,  $k = 2\pi/\lambda$  denotes the wave number,  $\lambda$  represents the wavelength,  $\psi(\mathbf{s}, \rho, L)$  corresponds to the complex random phase distortion caused by the spherical wave in the turbulent atmosphere from  $(\mathbf{s}, 0)$  to  $(\rho, L)$ ,  $*$  denotes the complex conjugate, and  $\langle \cdot \rangle$  represents the coefficient of integration averaged over the turbulent medium. If the stochastic medium is statistically homogeneous and isotropic, the  $\langle \cdot \rangle$  term can be expressed as [12]

$$\begin{aligned} & \langle \exp[\psi(\mathbf{s}_1, \rho_1, L) + \psi^*(\mathbf{s}_2, \rho_2, L)] \rangle \\ & = \exp \left[ -M[(\mathbf{s}_1 - \mathbf{s}_2)^2 + (\mathbf{s}_1 - \mathbf{s}_2)(\rho_1 - \rho_2) + (\rho_1 - \rho_2)^2] \right] \end{aligned} \tag{6}$$

where  $M = \frac{1}{3}\pi^2 k^2 L \int_0^\infty \kappa^3 \Phi_n(\kappa) d\kappa$ ,  $\Phi_n(\kappa)$  is the refractive index undulation spatial spectral density function of the turbulent medium, and here is the refractive index undulation spatial spectral density function of oceanic turbulence. Without considering the absorption and scattering of particles in the water, assuming that the oceanic turbulence is a locally uniform and isotropic, the spatial power spectral function of the oceanic turbulence can be expressed as [22]

$$\begin{aligned} \Phi_n(\kappa) & = 0.388 \times 10^{-8} \times \varepsilon^{-1/3} \kappa^{-11/3} [1 + 2.35(\kappa\eta)^{2/3}] \\ & \times \frac{\chi_T}{\omega^2} [\omega^2 \exp(-A_T\delta) + \exp(-A_S\delta) - 2\omega \exp(-A_{TS}\delta)] \end{aligned} \tag{7}$$

where  $\varepsilon$  is the turbulent kinetic energy dissipation rate per unit mass of fluid, taking the range of  $10^{-1} \sim 10^{-10} \text{ m}^2/\text{s}^3$ .  $\chi_T$  is the temperature variance dissipation rate, which takes values in the range of  $10^{-4} \sim 10^{-10} \text{ K}^2/\text{s}$  from the submerged surface to the deep water layer.  $\omega$  defines the relative ratio of temperature change to salinity change and takes values in the range of  $-5 \sim 0$ ,  $\omega = 0$  corresponds to salinity-dominated turbulence, and  $\omega = -5$  corresponds to temperature-dominated turbulence.  $\eta = 10^{-3} \text{ m}$  is the Kolmogorov microscale. The values of the other parameters are given below:

$$A_T = 1.863 \times 10^{-2}, A_S = 1.9 \times 10^{-4}, A_{TS} = 9.41 \times 10^{-3}, \delta = 8.284(\kappa\eta)^{4/3} + 12.987(\kappa\eta)^2$$

By substituting Equations (6) and (7) into Equation (5), we obtain [19]

$$\begin{aligned} W(\rho_1, \rho_2, L) & = \frac{P_n k^2 w_0^2}{8TL^2} \exp \left[ - \left( M + \frac{k^2 w_0^2}{8L^2} - \frac{\pi^2 Q^2}{T} \right) (\rho_1 - \rho_2)^2 \right] \\ & \times \exp \left[ - \frac{k^2}{16L^2 T} (\rho_1 + \rho_2)^2 \right] \exp \left[ - \frac{ik}{2L} \left( 1 - \frac{\pi Q}{T} \right) (\rho_1^2 - \rho_2^2) \right] \\ & \times \sum_{n=1}^N \sum_{m=1}^N \exp \left[ - \frac{k^2}{16L^2 T} (\mathbf{r}_n + \mathbf{r}_m)^2 \right] \exp \left[ \left( \frac{1}{4T\delta^4} - \frac{1}{2\delta^2} \right) ((\mathbf{r}_n - \mathbf{r}_m)^2) \right] \\ & \times \exp \left[ \frac{k^2}{8L^2 T} (\mathbf{r}_n + \mathbf{r}_m) \cdot (\rho_1 + \rho_2) \right] \exp \left[ \frac{\pi Q}{\delta^2 T} (\mathbf{r}_n - \mathbf{r}_m) \cdot (\rho_1 - \rho_2) \right] \\ & \times \exp \left[ \frac{ik}{2L} \left( 1 - \frac{\pi Q}{T} \right) (\mathbf{r}_n + \mathbf{r}_m) \cdot (\rho_1 - \rho_2) \right] \exp \left[ \frac{ik}{2L} \frac{(\mathbf{r}_n - \mathbf{r}_m) \cdot (\rho_1 + \rho_2)}{2\delta^2 T} \right] \end{aligned} \tag{8}$$

where  $\frac{1}{\delta^2} = \frac{1}{w_0^2} + \frac{1}{\sigma_0^2}$ ,  $T = \frac{1}{2\delta^2} + M + \frac{k^2 w_0^2}{8L^2}$ ,  $Q = \frac{k^2 w_0^2}{8\pi L^2} - \frac{M}{2\pi}$ . Combining the cross-spectral density functions of Equations (4) and (8), further analysis is conducted on the variations of average light intensity, array beamwidth, and spatial coherence.

When  $\rho_1 = \rho_2 = \rho$  in the cross-spectral density function of  $W(\rho_1, \rho_2, L)$ , the average light intensity of the radial PCLED beam array in oceanic turbulence can be obtained after transmitting a distance of  $L$  by considering the ocean attenuation and turbulence effects in combination with Equations (4) and (8):

$$\begin{aligned}
 \langle I(\boldsymbol{\rho}, L) \rangle &= W(\boldsymbol{\rho}, \boldsymbol{\rho}, L) \exp[(a + b)L] \\
 &= \frac{P_n k^2 w_0^2}{8TL^2} \exp\left[-\frac{k^2}{4L^2 T} \boldsymbol{\rho}^2\right] \sum_{n=1}^N \sum_{m=1}^N \left\{ \exp\left[-\frac{k^2}{16L^2 T} (\mathbf{r}_n + \mathbf{r}_m)^2\right] \right. \\
 &\times \exp\left[\left(\frac{1}{4T\delta^4} - \frac{1}{2\delta^2}\right) (\mathbf{r}_n - \mathbf{r}_m)^2\right] \exp\left[\frac{k^2}{4L^2 T} (\mathbf{r}_n + \mathbf{r}_m) \cdot \boldsymbol{\rho}\right] \exp\left[\frac{ik}{2L\delta^2 T} (\mathbf{r}_n - \mathbf{r}_m) \cdot \boldsymbol{\rho}\right] \left. \right\} \\
 &\times \exp[(a + b)L]
 \end{aligned} \tag{9}$$

The values of the other parameters are the same as mentioned above.

According to the definition of the second-order moment beamwidth, the second-order moment beamwidth of the radial PCLED beam array can be expressed as [22]

$$w(L) = \left[ \frac{2 \iint \boldsymbol{\rho}^2 I(\boldsymbol{\rho}, L) d^2 \boldsymbol{\rho}}{\iint I(\boldsymbol{\rho}, L) d^2 \boldsymbol{\rho}} \right]^{1/2} \tag{10}$$

Substituting Equation (9) into Equation (10) and rearranging, we obtain

$$w(L) = \left[ \frac{\sum_{m=1}^N \sum_{n=1}^N \exp\left[-\frac{(\mathbf{r}_n - \mathbf{r}_m)^2}{2\delta^2}\right] \left[ \frac{(\mathbf{r}_n + \mathbf{r}_m)^2}{2} - \frac{2L^2 (\mathbf{r}_n - \mathbf{r}_m)^2}{k^2 \delta^4} + \frac{8TL^2}{k^2} \right]}{\sum_{m=1}^N \sum_{n=1}^N \exp\left[-\frac{(\mathbf{r}_n - \mathbf{r}_m)^2}{2\delta^2}\right]} \right]^{1/2} \tag{11}$$

The spatial coherence plays a crucial role in characterizing the effects of turbulence on beam propagation and in optical adaptive phase correction techniques. Therefore, studying the spatial coherence characteristics of the radial PCLED beam array in oceanic turbulence is of significant importance. Typically, the complex spatial coherence coefficient  $\mu(\boldsymbol{\rho}_1, \boldsymbol{\rho}_2, L)$  [23] is introduced to represent the spatial coherence of the beam. For convenience, we consider the spatial coherence between any point on the receiving plane and the optical axis, where  $\boldsymbol{\rho}_1 = \boldsymbol{\rho}$  and  $\boldsymbol{\rho}_2 = 0$ . In this case, the spatial coherence coefficient of the beam can be expressed as

$$|\mu(\boldsymbol{\rho}, 0, L)| = \frac{|W(\boldsymbol{\rho}, 0, L)|}{\sqrt{W(\boldsymbol{\rho}, \boldsymbol{\rho}, L)W(0, 0, L)}} \tag{12}$$

By substituting Equation (8) into Equation (12), we can derive the expression for the complex spatial coherence of the PCLED beam array during its propagation in oceanic turbulence as

$$\begin{aligned}
 |\mu(\boldsymbol{\rho}, 0, L)| &= \exp\left[-\left(M + \frac{k^2 w_0^2}{8L^2} - \frac{\pi^2 Q^2}{T} - \frac{k^2}{16L^2 T} + \frac{ik}{2L} - \frac{ik\pi Q}{2LT}\right) \boldsymbol{\rho}^2\right] \\
 &\times \exp\left\{\left[\frac{\pi Q}{\delta^2 T} (\mathbf{r}_n - \mathbf{r}_m) + \frac{ik}{2L} \left(1 - \frac{\pi Q}{T}\right) (\mathbf{r}_n + \mathbf{r}_m)\right] \cdot \boldsymbol{\rho}\right\}
 \end{aligned} \tag{13}$$

In summary, the next section will delve into a comprehensive analysis of how the spatial coherence of sub-beams, attenuation parameters, and turbulence parameters impact the average light intensity distribution, beam width, and spatial coherence of the radial PCLED beam array during its propagation in the ocean.

### 3. Simulated Results and Corresponding Discussion

In this section, we conduct numerical simulations to analyze the transmission characteristics and spatial coherence of the PCLED array in the ocean. In practical applications, the analyses of the optical field and photons in array beam transmission complement each other based on the specific application requirements. As the intensity decreases to

the nanowatt level ( $10^{-9} \text{ W/m}^2$ ) or below, only a small number of photons pass through, requiring consideration of the discreteness and quantum nature of photons. Consequently, the description of the optical field may no longer be applicable. For our simulations, we choose a maximum distance of  $L = 150 \text{ m}$  and the peak magnitude of the average light intensity distribution is on the order of  $10^{-5} \text{ W/m}^2$ . The sub-beam is selected from the widely used green light in the underwater blue-green light band. Moreover, we set the parameter values based on typical values, as shown in Table 1.

**Table 1.** Parameter Settings.

Parameters	Values	Parameters	Values	Parameters	Values
$\lambda/\text{nm}$	525 [24]	$w_0/\text{m}$	0.01	$P_0/\text{W/m}^2$	6.4 [25]
$N$	8	$NP_0/\text{W/m}^2$	51.2	$r_0/w_0$	3
$a/\text{m}^{-1}$	0.053	$b/\text{m}^{-1}$	0.003	$c/\text{m}^{-1}$	0.056
$\varepsilon/\text{m}^2/\text{s}^3$	$10^{-5}$	$\chi_T/\text{K}^2/\text{s}$	$10^{-7}$	$\omega$	-2.5

### 3.1. Average Light Intensity

The experimental LED measurements of the spatial coherence lengths were performed using classical techniques as described in [11,15,26]. Additionally, controlling LED-based sources, as outlined in [27,28], could be utilized to obtain the spatial coherence length. Based on the collective data, we carefully selected two specific spatial coherence lengths,  $\sigma_0 = 500 \mu\text{m}$  and  $\sigma_0 = 50 \mu\text{m}$ , representing typical sub-beams for further analysis. By incorporating Equation (9) and conducting numerical analysis using Figures 2–4, we examine the influence of transmission distance  $L$ , attenuation parameters, turbulence parameters, and light source parameters on the average light intensity of the radial PCLED beam array during its propagation in oceanic turbulence.

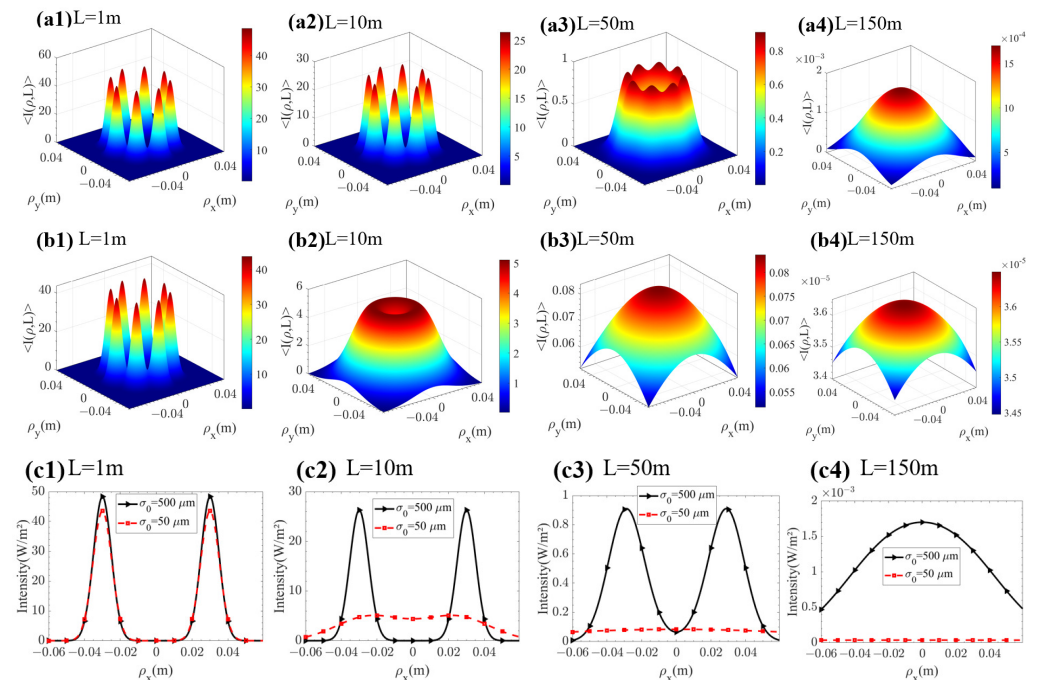


**Figure 2.** Average light intensity of radial PCLED beam array at different transmission distances. (a)  $\sigma_0 = 500 \mu\text{m}$ . (b)  $\sigma_0 = 50 \mu\text{m}$ . (c) Cross-sectional intensity distribution ( $\rho_y = 0$ ).

Figure 2 presents the impact of different  $L$  on the average light intensity of the radial PCLED beam array during its propagation in the ocean. The values of other parameters remain consistent with those specified in Table 1. The figure reveals that for shorter transmission distances, the light intensity distribution of the beam array displays multiple

peaks. As the transmission distance increases, the effects of attenuation and turbulence on the beam array become more pronounced, resulting in the spreading and overlapping of sub-beams. Consequently, the on-axis light intensity gradually increases, leading to a more concentrated energy distribution. For  $\sigma_0 = 500 \mu\text{m}$  and  $\sigma_0 = 50 \mu\text{m}$ , at a transmission distance of  $L = 1 \text{ m}$ , the beam array attains a maximum light intensity of approximately  $40 \text{ W/m}^2$ . As the spatial coherence length decreases, the light intensity distribution degrades into a Gaussian-like distribution earlier as the distance increases, accompanied by a notable reduction in peak intensity. The beam spreading of the converging beam becomes more prominent. For a transmission distance of 10m, the peak intensities decrease to  $26.17 \text{ W/m}^2$  and  $5.11 \text{ W/m}^2$  for  $\sigma_0 = 500 \mu\text{m}$  and  $\sigma_0 = 50 \mu\text{m}$ , respectively. This demonstrates that the intensity distribution of the beam array is significantly influenced by water attenuation and turbulence parameters. Further analysis is provided in Figures 3 and 4.

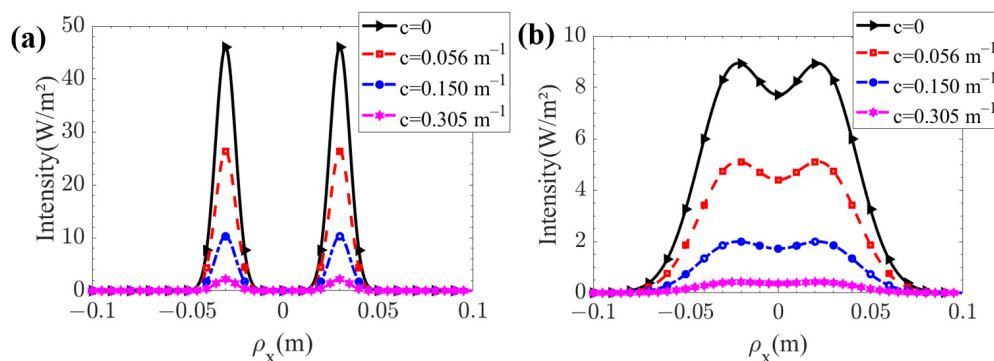


**Figure 3.** Average light intensity of radial PCLED beam array at different attenuation coefficients ( $L = 10 \text{ m}$ ). (a)  $\sigma_0 = 500 \mu\text{m}$ . (b)  $\sigma_0 = 50 \mu\text{m}$ .

To provide a clearer understanding of the influence of different water attenuation coefficients on the beam array, a transmission distance of  $L = 10 \text{ m}$  is selected. Figure 3 illustrates the average light intensity of the radial PCLED beam array propagated through oceanic turbulence for water attenuation coefficients of  $0 \text{ m}^{-1}$ ,  $0.056 \text{ m}^{-1}$ ,  $0.150 \text{ m}^{-1}$ , and  $0.305 \text{ m}^{-1}$  in different water types [21]. The other parameters remain the same as Table 1. From the figure, it is evident that under the conditions of  $\sigma_0 = 500 \mu\text{m}$  and  $\sigma_0 = 50 \mu\text{m}$ , the impact of various attenuation coefficients on the beam array after normalization is proportionally the same. As the water attenuation coefficient increases, the average light intensity along the optical transmission path of the PCLED beam array notably decreases. For  $\sigma_0 = 500 \mu\text{m}$ , the maximum light intensity values of the PCLED beam array corresponding to different attenuation coefficients are  $46.02 \text{ W/m}^2$ ,  $26.28 \text{ W/m}^2$ ,  $10.22 \text{ W/m}^2$ , and  $2.17 \text{ W/m}^2$ , respectively. In the case of  $\sigma_0 = 50 \mu\text{m}$ , the maximum light intensity values are  $8.94 \text{ W/m}^2$ ,  $5.10 \text{ W/m}^2$ ,  $1.99 \text{ W/m}^2$ , and  $0.42 \text{ W/m}^2$ , respectively. This finding confirms that the water attenuation coefficient affects the average intensity distribution of the beam array, independent of the spatial coherence of the sub-beams within the light source.

To provide a more comprehensive understanding of the influence of turbulence parameters on the average light intensity of the radial PCLED beam array, Figure 4 depicts the average light intensity at a transmission distance of  $L = 50 \text{ m}$  for various values of kinetic energy dissipation rate  $\epsilon$ , temperature dissipation rate  $\chi_T$ , temperature-to-salinity ratio  $\omega$ , as well as the sub-beam spatial coherence length  $\sigma_0$ . The values of the other parameters are given in Table 1. From the analysis of Figure 4a,b, it is evident that as the value of  $\epsilon$  decreases, indicating larger turbulence scales and increased turbulence intensity [29], the impact on the average light intensity of the PCLED beam array becomes less significant. In the case of  $\epsilon = 10^{-3}$ ,  $10^{-5}$ , and  $10^{-7} \text{ m}^2/\text{s}^3$  shown in Table 2, the light intensity distribution gradually transitions from a multi-peak distribution to a Gaussian-like distribution. This observation reveals that as the  $\epsilon$  changes on the order of micrometers,

the peak intensity of the beam array diminishes by approximately a factor of 12. Based on Figure 4(a2,b2), with an increase in  $\chi_T$ , there is a substantial augmentation in turbulence intensity, resulting in notable alterations in both the distribution and peak intensity of light. This escalation signifies a more active oceanic turbulence [30]. Notably, the impact on the array’s light intensity distribution is more pronounced when the  $\sigma_0$  is larger. Based on Figure 4(c3,b3), as  $\omega$  increases, there is a gradual decrease in the peak intensity of the array beams, accompanied by a transition in the light intensity distribution from a multi-peak pattern to a Gaussian-like distribution. This degradation is particularly prominent when  $\sigma_0$  is smaller.

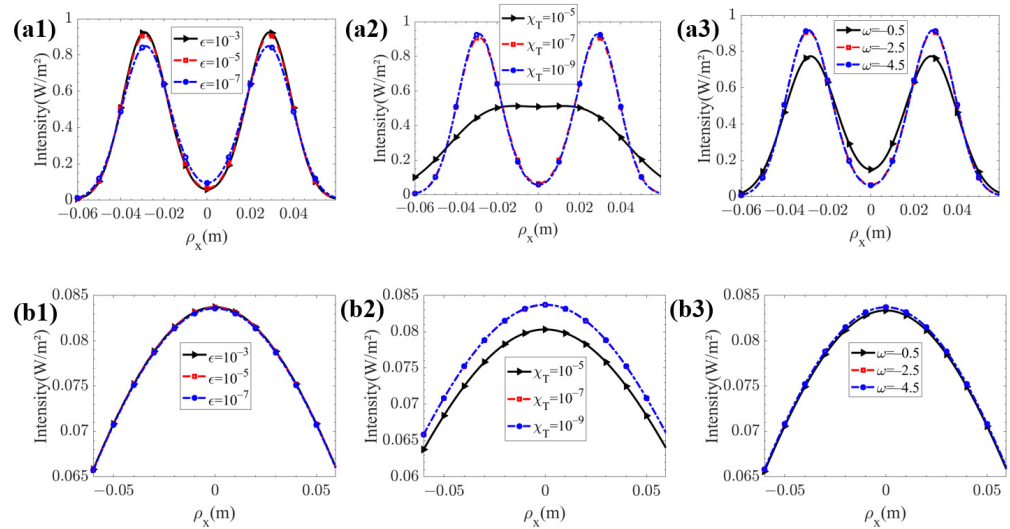


**Figure 4.** Average light intensity of radial PCLED beam array at different oceanic turbulence parameters ( $L = 50$  m). (a)  $\sigma_0 = 500 \mu\text{m}$ . (b)  $\sigma_0 = 50 \mu\text{m}$ .

**Table 2.** Peak intensities ( $\text{W}/\text{m}^2$ ) for different turbulence parameters and  $\sigma_0$  ( $L = 50$  m).

$\sigma_0/\mu\text{m}$	$\epsilon/\text{m}^2/\text{s}^3$			$\chi_T/\text{K}^2/\text{s}$			$\omega$		
	$10^{-3}$	$10^{-5}$	$10^{-7}$	$10^{-5}$	$10^{-7}$	$10^{-9}$	$-0.5$	$-2.5$	$-4.5$
500	0.93	0.91	0.85	0.51	0.91	0.93	0.77	0.91	0.92
50	0.080	0.080	0.080	0.080	0.083	0.083	0.083	0.083	0.083

To further analyze the impact of  $\sigma_0$  on the array beams, Figure 5 illustrates the variations in the average light intensity of the radial PCLED array beams at a distance of  $L = 50$  m for different  $\sigma_0$ . When  $\sigma_0 = 5000$ , the light source can be approximated as a laser array, and while  $\sigma_0 = 0$ , the light source can be regarded as a fully incoherent light array. The curves overlap as for  $\sigma_0$  values of  $50 \mu\text{m}$  and  $0$ . As observed from the graph, when  $\sigma_0$  is smaller, the average light intensity of the array beams is influenced by attenuation and turbulence along the oceanic transmission path. Not only does it achieve combining of sub-beams earlier, but it also results in a larger combining spot size. For the aforementioned parameter values of  $\sigma_0$ , the peak light intensity of the radial PCLED array beams is  $0.77 \text{ W}/\text{m}^2$ ,  $0.91 \text{ W}/\text{m}^2$ , and  $0.92 \text{ W}/\text{m}^2$ , respectively. This finding aligns with conclusions drawn from underwater experimental studies, where LEDs with smaller  $\sigma_0$  values exhibit closer underwater light transmission distances and larger beam spreading compared to lasers with larger  $\sigma_0$  values [29].

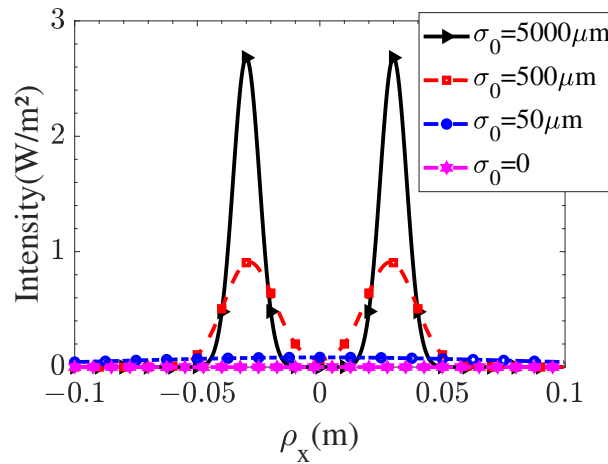


**Figure 5.** Average light intensity of radial PCLED beam array at different  $\sigma_0$  ( $L = 50$  m).

The radial fill factor parameter, denoted as  $r_0/w_0$ , is introduced to quantify the compactness of the beam array arrangement. A smaller value indicates a tighter arrangement of the beams, with  $r_0/w_0 \geq 1$ . Figure 6 illustrates the light intensity distribution of the PCLED beam array at the observation plane of  $L = 10$  m for various  $r_0/w_0$ . When  $\sigma_0 = 500 \mu\text{m}$ , the peak light intensities of the radial PCLED beam array are  $26.28 \text{ W/m}^2$ ,  $27.09 \text{ W/m}^2$ , and  $48.95 \text{ W/m}^2$  for  $r_0/w_0$  values of 3, 2, and 1, respectively. When  $\sigma_0 = 50 \mu\text{m}$ , the peak light intensities of the array are  $5.11 \text{ W/m}^2$ ,  $10.01 \text{ W/m}^2$ , and  $16.38 \text{ W/m}^2$ , respectively. As  $r_0/w_0$  increases, the peak light intensity decreases, accompanied by the dispersion of beam energy and a spreading effect on the array beam. This reduction in intensity is a consequence of decreased coherence between the sub-beams, arising not only from the spatial coherence length of the individual sub-beams but also from the decreased compactness of the beam array arrangement as a whole.

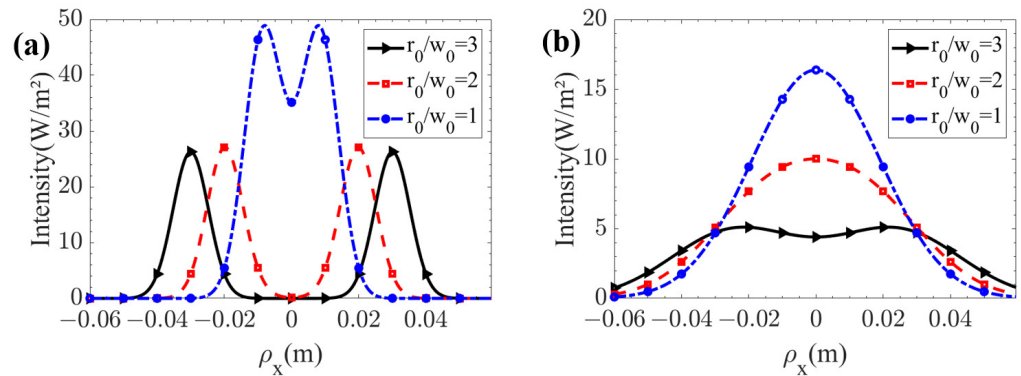


**Figure 6.** Average light intensity of radial PCLED beam array at different radial fill factors ( $L = 10$  m). (a)  $\sigma_0 = 500 \mu\text{m}$ . (b)  $\sigma_0 = 50 \mu\text{m}$ .

### 3.2. Array Beam Width

Numerical simulations of the average light intensity reveal that the water attenuation coefficient does not cause beam spreading. Combining with Equation (12), Figures 7 and 8 numerically analyze the effects of the turbulence parameters of  $\epsilon$ ,  $\chi_T$ ,  $\omega$ , and  $\sigma_0$  on the beam width of the radial PCLED beam array in oceanic turbulence. The remaining parameters are set as described in Table 1.

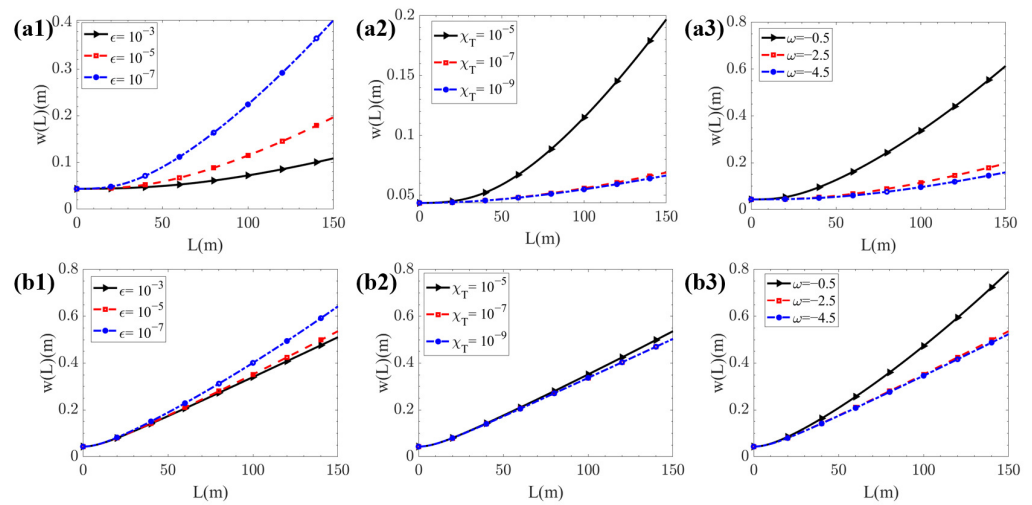


**Figure 7.** Variation of radial PCLED array beam width with transmission distance at different turbulence parameters. (a)  $\sigma_0 = 500 \mu\text{m}$ . (b)  $\sigma_0 = 50 \mu\text{m}$ .

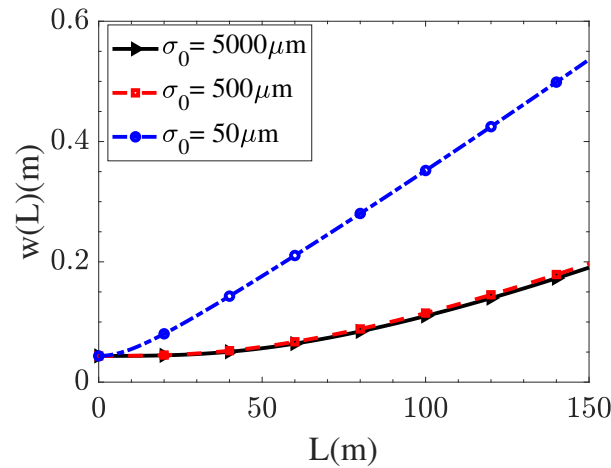


**Figure 8.** Variation of radial PCLED array beam width with transmission distance at different  $\sigma_0$ .

Figure 7 depicts the changes in the beam width of the radial PCLED beam array as  $L$  increases under different turbulence parameters. From the graph, it is evident that for  $\sigma_0 = 500 \mu\text{m}$  and  $\sigma_0 = 50 \mu\text{m}$ , the array beam undergoes varying degrees of spreading under different turbulence conditions. Specifically, Figure 7a shows a gradual change in the array beam width starting from  $L = 7 \text{ m}$ , while Figure 7b indicates that the array beam width experiences changes from  $L = 0 \text{ m}$ . As the turbulence parameter  $\epsilon$  decreases,  $\omega$  increases, and  $\chi_T$  increases, array beam spreading becomes more pronounced, shown in Table 3. Specially, when  $\chi_T$  is  $10^{-7} \text{ K}^2/\text{s}$  or  $10^{-9} \text{ K}^2/\text{s}$ , the array width is affected by turbulence to almost the same extent. However, at  $\chi_T = 10^{-5} \text{ K}^2/\text{s}$  and  $\sigma_0$  values of  $500 \mu\text{m}$  and  $50 \mu\text{m}$ , the array widths are  $0.197 \text{ m}$  and  $0.536 \text{ m}$ , respectively. In brief, the spreading effect of the radial PCLED array beam width is mainly influenced by the turbulence parameters  $\epsilon$  and  $\omega$ , while the influence of  $\chi_T$  is relatively smaller. Additionally, a smaller value of  $\sigma_0$  leads to a reduced spreading effect.

To further investigate the impact of  $\sigma_0$  on the array width, Figure 8 depicts the variations in the beam width of the radial PCLED array for  $\sigma_0$  values of  $5000 \mu\text{m}$ ,  $500 \mu\text{m}$ , and  $50 \mu\text{m}$ . From the graph, it can be observed that as the value of  $\sigma_0$  decreases, the beam width increases. Specifically, for the mentioned parameter values of  $\sigma_0$ , the array beam width starts changing from  $L = 10 \text{ m}$ ,  $L = 7 \text{ m}$ , and  $L = 0 \text{ m}$ , respectively. At the observation plane located at  $L = 150 \text{ m}$ , the corresponding beam widths are measured as  $L = 0.533 \text{ m}$ ,  $L = 0.193 \text{ m}$ , and  $L = 0.191 \text{ m}$ . When considering practical engineering

applications, it becomes crucial to select an appropriate value of  $\sigma_0$  based on specific requirements. This finding emphasizes the significance of accounting for beam spreading in LED array systems and highlights their advantages in short-range directional transmission and positioning applications.

**Table 3.**  $w(L)$  (m) for different turbulence parameters and  $\sigma_0$  ( $L = 150$  m).

$\sigma_0/\mu\text{m}$	$\epsilon/\text{m}^2/\text{s}^3$			$\chi_T/\text{K}^2/\text{s}$			$\omega$		
	$10^{-3}$	$10^{-5}$	$10^{-7}$	$10^{-5}$	$10^{-7}$	$10^{-9}$	-0.5	-2.5	-4.5
500	0.109	0.197	0.405	0.197	0.069	0.066	0.613	0.197	0.159
50	0.511	0.536	0.642	0.536	0.504	0.503	0.791	0.536	0.524

Figure 9 illustrates the variations in the beam width of the radial PCLED beam array in oceanic turbulence with increasing  $L$  for different values of  $r_0/w_0$ , with other parameters as listed in Table 1. From the graph, it can be observed that as  $\sigma_0$  decreases, the spreading of the array beam becomes more pronounced. Particularly at the observation plane of  $L = 150$  m, when  $r_0/w_0 = 3$ , the beam width of the radial PCLED beam array is 2.8 times larger for  $\sigma_0 = 50 \mu\text{m}$  compared to  $\sigma_0 = 500 \mu\text{m}$ . When  $\sigma_0 = 50 \mu\text{m}$ , the beam width variations of the array overlap for different radial fill factors after  $L = 20$  m.

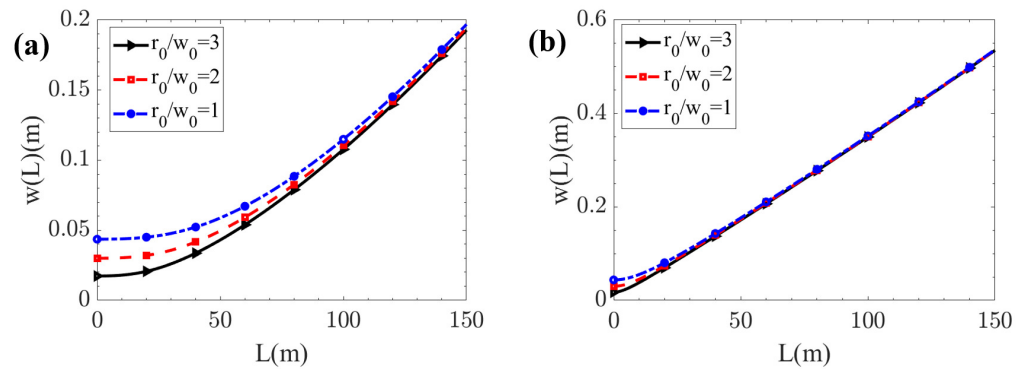


**Figure 9.** Variation of radial PCLED array beam width with transmission distance at different  $r_0/w_0$ . (a)  $\sigma_0 = 500 \mu\text{m}$ . (b)  $\sigma_0 = 50 \mu\text{m}$ .

### 3.3. Spatial Coherence

Investigating the spatial coherence of the received array beam section not only enhances system performance and reliability but also improves interference resistance, enables precise beam management and control, and provides guidance for antenna design and optimization. By utilizing Equation (13), it is possible to analyze the changes in the spatial coherence of the PCLED beam array in the oceanic transmission path. This analysis takes into account  $L$ ,  $\sigma_0$ , turbulence parameters, and  $r_0/w_0$ .

To comprehensively analyze the variation patterns of  $|\mu|$ , Figure 10 illustrates the changes in  $|\mu|$  as  $L$  increases for different values of  $\sigma_0$ . To illustrate the comparison of results, the values of  $\sigma_0$  are introduced as  $5000 \mu\text{m}$ ,  $500 \mu\text{m}$ , and  $50 \mu\text{m}$ , respectively. By setting  $|\mu| = 1/e \approx 0.368$ , the corresponding values of  $\rho_0$  can be obtained, enabling the determination of the variation patterns of  $|\mu|$  on the observation plane with increasing distance. From the graph, it is evident that as  $\rho_x$  varies,  $|\mu|$  exhibits a multi-peak phenomenon. For  $L$  values of  $50$  m,  $100$  m, and  $150$  m, when  $\sigma_0 = 5000 \mu\text{m}$ , the corresponding values of  $\rho_0$  are  $1.09$  mm,  $0.60$  mm, and  $0.60$  mm, respectively. When  $\sigma_0 = 500 \mu\text{m}$ , the values of  $\rho_0$  are  $0.31$  mm,  $0.48$  mm, and  $0.65$  mm, and when  $\sigma_0 = 50 \mu\text{m}$ , the values of  $\rho_0$  are  $0.23$  mm,  $0.46$  mm, and  $0.67$  mm. This indicates that under the given conditions of oceanic turbulence parameters, when the transmission distance is relatively short, the free-space diffraction effect of the beam is stronger than the turbulence effect, resulting in an increased distribution width of  $|\mu|$ . As  $L$  increases, the cumulative effect of turbulence becomes more

pronounced. However, due to the relatively small value of  $\sigma_0$ , the turbulence effect does not dominate the variation in the distribution of  $|\mu|$ . As a result, the coherence of the beam is minimally affected, and the distribution width of  $|\mu|$  continues to increase. This finding suggests that the spatial coherence of PCLED arrays is less affected by turbulence in the oceanic transmission path compared to laser arrays discussed in literatures.

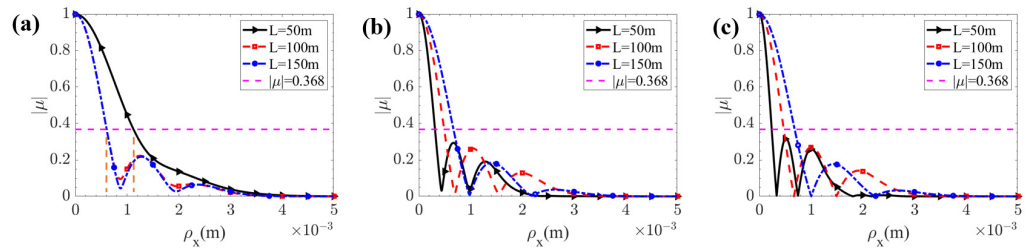


**Figure 10.** Spatial coherence of the radial PCLED beam array varies with different  $L$ . (a)  $\sigma_0 = 5000 \mu\text{m}$ . (b)  $\sigma_0 = 500 \mu\text{m}$ . (c)  $\sigma_0 = 50 \mu\text{m}$ .

To investigate the impact of turbulence parameters on the spatial coherence of the array beams for different  $\sigma_0$  values, Figure 11 depicts the variations of  $|\mu|$  at the observation plane with  $L = 150 \text{ m}$ , considering  $\sigma_0$  values of  $5000 \mu\text{m}$ ,  $500 \mu\text{m}$ , and  $50 \mu\text{m}$ , and the specific values of  $\rho_0$  are shown in Table 4. From Figure 11a–c, it can be observed that as  $\omega$  and  $\chi_T$  increase and  $\epsilon$  decreases, the beam width  $\rho_0$  of the array gradually narrows, indicating a degradation of spatial coherence. The distribution of the beam’s spatial coherence evolves from a multi-peak distribution to a Gaussian distribution.

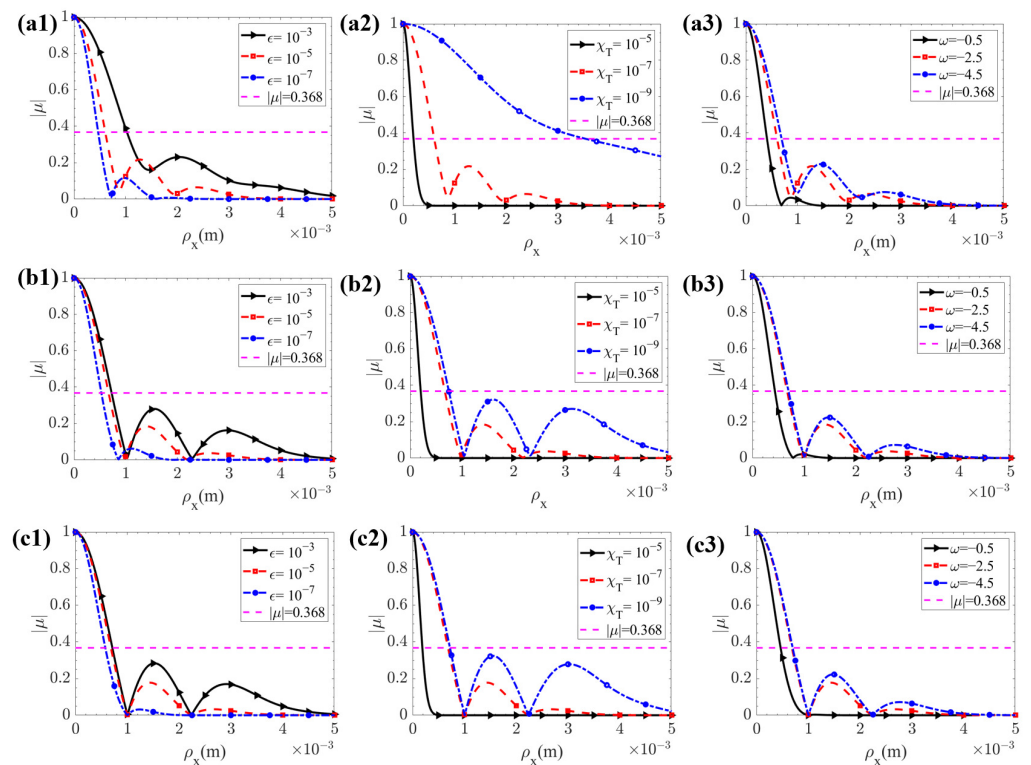
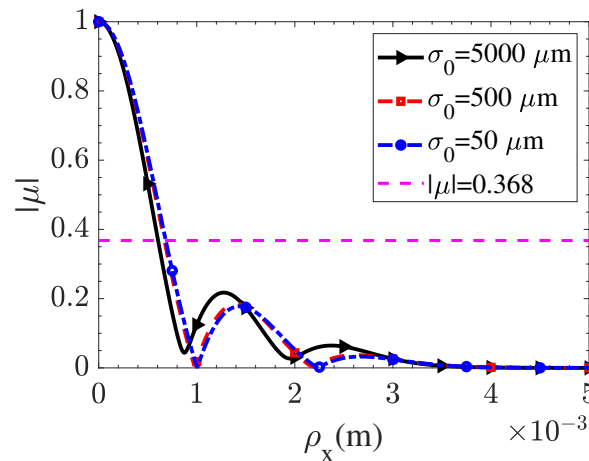


**Figure 11.** Spatial coherence of the radial PCLED beam array varies with different turbulence parameters ( $L = 150 \text{ m}$ ). (a)  $\sigma_0 = 5000 \mu\text{m}$ . (b)  $\sigma_0 = 500 \mu\text{m}$ . (c)  $\sigma_0 = 50 \mu\text{m}$ .

**Table 4.**  $\rho_0$  (mm) for different turbulence parameters and  $\sigma_0$  ( $L = 150$  m).

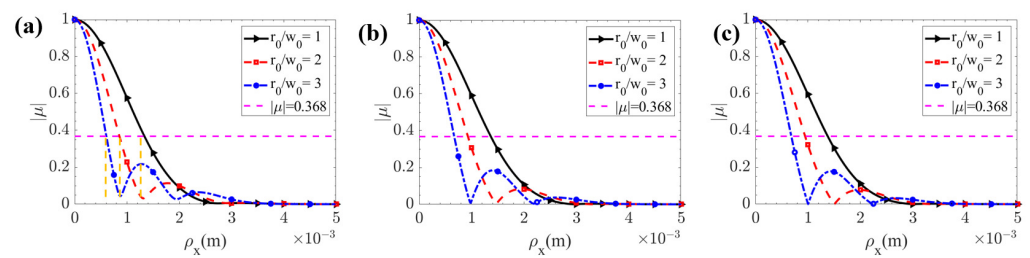
$\sigma_0/\mu\text{m}$	$\epsilon/\text{m}^2/\text{s}^3$			$\chi_T/\text{K}^2/\text{s}$			$\omega$		
	$10^{-3}$	$10^{-5}$	$10^{-7}$	$10^{-5}$	$10^{-7}$	$10^{-9}$	-0.5	-2.5	-4.5
5000	1.01	0.60	0.45	0.20	0.60	3.44	0.40	0.60	0.68
500	0.72	0.66	0.52	0.20	0.66	0.73	0.42	0.68	0.68
50	0.70	0.68	0.56	0.18	0.67	0.68	0.46	0.68	0.68

Figure 12 illustrates the impact of different  $\sigma_0$  on the spatial coherence distribution of radial PCLED array beams at the observation plane of  $L = 150$  m. The remaining parameters are consistent with those specified in Table 1. The graph demonstrates that increasing the value of  $\sigma_0$  leads to a decrease in  $\rho_0$ , with the values approaching each other. Specifically, when  $\sigma_0$  is set to 5000  $\mu\text{m}$ , 500  $\mu\text{m}$ , and 50  $\mu\text{m}$ , the corresponding values of  $\rho_0$  are 0.60 mm, 0.67 mm, and 0.68 mm, respectively. Combining this information with the preceding average intensity distribution, it becomes evident that the micrometer level of  $\sigma_0$  for PCLED array itself exhibit a dampening effect on the oceanic turbulence phenomenon at observation planes characterized by relatively low light intensities.



**Figure 12.** Spatial coherence of the radial PCLED beam array varies with different  $\sigma_0$  ( $L = 150$  m).

To further analyze the influence of the radial filling factor of the light source on the spatial coherence of the array, Figure 13 illustrates the variation curve of the beam array’s spatial coherence at the observation plane with  $L = 150$  m. The graph reveals that an increasing value of  $r_0/w_0$  leads to a more dispersed arrangement of the beams, resulting in a significant reduction in the width of the  $|\mu|$  value distribution. Moreover, the distribution of the array’s spatial coherence exhibits oscillations with multiple peaks as the distance from the axis increases. However, at the observation plane with  $L = 150$  m, where the light intensity is relatively weak, the variation in the spatial coherence of the beam array is not obvious. When considering  $r_0/w_0$  values of 1, 2, and 3, with  $\sigma_0 = 5000 \mu\text{m}$ , the corresponding  $\rho_0$  values are 1.32 mm, 0.84 mm, and 0.60 mm, respectively. When  $\sigma_0 = 500 \mu\text{m}$ , the  $\rho_0$  values are 1.35 mm, 0.92 mm, and 0.66 mm, respectively. When  $\sigma_0 = 50 \mu\text{m}$ , the  $\rho_0$  values are 1.35 mm, 0.94 mm, and 0.68 mm, respectively. These findings indicate that the radial PCLED beam array itself possesses the ability to suppress turbulence effects during oceanic transmission. Furthermore, by optimizing diversity reception, the application of LED array light sources can be extended beyond close-range high-speed transmission purposes, such as underwater communication and imaging.



**Figure 13.** Spatial coherence of the radial PCLED beam array varies with different  $r_0/w_0$ . (a)  $\sigma_0 = 5000 \mu\text{m}$ . (b)  $\sigma_0 = 500 \mu\text{m}$ . (c)  $\sigma_0 = 50 \mu\text{m}$ .

#### 4. Conclusions

This paper comprehensively considers channel parameters such as water attenuation coefficient, kinetic dissipation rate, temperature dissipation rate, and the ratio of temperature to salinity, as well as light source parameters such as radial filling factor and sub-beam spatial coherence length. By combining the high-order Lambertian model, an analytical expression for the radial PCLED beam array is established. Based on the extended Huygens–Fresnel integral, the theoretical research investigates the influence of these parameters on the average intensity distribution, beam width, and spatial coherence of the radial PCLED beam array. The research findings indicate that as the sub-beam spatial coherence length decreases from  $\sigma_0 = 500 \mu\text{m}$  to  $\sigma_0 = 50 \mu\text{m}$ , the beam-combining distance of the PCLED beam array decreases. As the distance increases, the intensity distribution degrades into a Gaussian-like distribution, and the peak intensity significantly decreases by a factor of 5. The array width expands from  $L = 7 \text{ m}$  and  $L = 0 \text{ m}$  at the respective transmission distances. Due to the micrometer-level spatial coherence length of the sub-beams, the radial PCLED beam array exhibits the characteristic of suppressing turbulence effects. Furthermore, it enables the research of high-speed real-time transmission in short-range underwater scenarios. Additionally, this study provides a theoretical foundation for future research on experimental channel analysis for real-time underwater LED transmission.

**Author Contributions:** X.H. and Z.M. proposed the project. Z.M. and F.L. conducted the equation derivation and simulation. Z.M. and X.H. wrote the manuscript. Q.W. and Q.L. helped to modify the documentation. All authors have read and agreed to the published version of the manuscript.

**Funding:** This work was supported by the Fundamental Research Funds for the Central Universities ZYTS23077, ZYTS23073.

**Institutional Review Board Statement:** Not applicable.

**Informed Consent Statement:** Not applicable.

**Data Availability Statement:** The original contributions presented in the study are included in the article; further inquiries can be directed to the corresponding authors.

**Conflicts of Interest:** The authors declare that the research was conducted in the absence of any commercial or financial relationships that could be construed as a potential conflict of interest.

#### References

1. Liu W.; Zhang, L.; Huang, N. Wide dynamic range signal detection for underwater optical wireless communication using a PMT detector. *Opt. Express* **2023**, *31*, 25267–25279. [[CrossRef](#)] [[PubMed](#)]
2. Zhu, S.; Chen, X.; Liu, X. Recent progress in and perspectives of underwater wireless optical communication. *Prog. Quantum Electron.* **2020**, *73*, 100273. [[CrossRef](#)]
3. Nikishov, V.V.; Nikishov, V.I. Spectrum of turbulent fluctuations of the sea-water refraction index. *Int. J. Fluid Mech. Res.* **2000**, *27*, 82–98. [[CrossRef](#)]
4. Cai, R.; Zhang, M.; Dai, D. Analysis of the underwater wireless optical communication channel based on a comprehensive multiparameter model. *Appl. Sci.* **2021**, *11*, 6051. [[CrossRef](#)]
5. Liu, D.; Wang, G.; Yin, H.; Zhong, H.; Wang, Y. Propagation properties of a partially coherent anomalous hollow vortex beam in underwater oceanic turbulence. *Opt. Commun.* **2019**, *437*, 346–354. [[CrossRef](#)]

6. Liu, L.; Liu, Y.; Chang, H.; Huang, J.; Zhu, X. Second-Order Statistics of Self-Splitting Structured Beams in Oceanic Turbulence. *Photonics* **2023**, *10*, 339. [[CrossRef](#)]
7. Liu, D.; Wang, Y. Evolution properties of a radial phased-locked partially coherent Lorentz-Gauss array beam in oceanic turbulence. *Opt. Laser Technol.* **2018**, *103*, 33–41. [[CrossRef](#)]
8. Liu, D.; Zhong, H.; Wang, G. Radial phased-locked multi-Gaussian Schell-model beam array and its properties in oceanic turbulence. *Opt. Laser Technol.* **2020**, *124*, 106003. [[CrossRef](#)]
9. Mao, Y.; Mei, Z.; Gu, J. Radial Gaussian-Schell-model array beams in oceanic turbulence. *Appl. Phys. B* **2017**, *123*, 111. [[CrossRef](#)]
10. Carter, W.H.; Wolf, E. Coherence properties of lambertian and non-lambertian sources. *J. Opt. Soc. Am.* **1975**, *65*, 1067–1071. [[CrossRef](#)]
11. Deng, Y.; Chu, D. Coherence properties of different light sources and their effect on the image sharpness and speckle of holographic displays. *Sci. Rep.* **2017**, *7*, 5893. [[CrossRef](#)] [[PubMed](#)]
12. Kong, M.; Kang, C.H.; Alkhazragi, O. Survey of energy-autonomous solar cell receivers for satellite–air–ground–ocean optical wireless communication. *Prog. Quantum Electron.* **2020**, *74*, 100300. [[CrossRef](#)]
13. Chen, Y.; Zhang, L. New approach for designing an underwater free-space optical communication system. *Front. Mar. Sci.* **2022**, *50*, 752–759. [[CrossRef](#)]
14. Petrov, N.I.; Petrova, G.N. Diffraction of partially-coherent light beams by microlens arrays. *Opt. Express* **2017**, *25*, 22545–22564. [[CrossRef](#)] [[PubMed](#)]
15. Xie, G.; Chen, M.; Mazilu, M. Measuring and structuring the spatial coherence length of organic light-emitting diodes. *Laser Photonics Rev.* **2016**, *20*, 82–90. [[CrossRef](#)]
16. Shen, S.C.; Kuo, C.Y.; Fang, M.C. Design and analysis of an underwater white LED fish-attracting lamp and its light propagation. *Int. J. Adv. Robot. Syst.* **2013**, *10*, 183. [[CrossRef](#)]
17. Miao, Z.; Zhang, P.; Lu, F.; Han, X.; Li, Q. Light field analysis for modeling and transmission characteristics of partially coherent light-emitting diodes. *Front. Phys.* **2023**, *11*, 1181343. [[CrossRef](#)]
18. Duarte, F.J.; Liao, L.S.; Vaeth, K.M. Coherence characteristics of electrically excited tandem organic light-emitting diodes. *Opt. Lett.* **2005**, *30*, 3072–3074. [[CrossRef](#)]
19. Lu, F.; Han, X. Spatial coherence properties of GSM array beams in turbulent atmosphere. *Infrared Laser Eng.* **2015**, *44*, 305–309.
20. Mobley, C.D.; Gentili, B.; Gordon, H.R. Comparison of numerical models for computing underwater light fields. *Appl. Opt.* **1993**, *32*, 484–7504. [[CrossRef](#)]
21. Zeng, Z.; Fu, S.; Zhang, H.; Dong, Y.; Cheng, J. A Survey of Underwater Optical Wireless Communications. *IEEE Commun. Surv. Tutor.* **2017**, *19*, 204–238. [[CrossRef](#)]
22. Carter, W. Spot size and divergence for Hermite Gaussian beams of any order. *Appl. Opt.* **1980**, *1*, 1027–1029. [[CrossRef](#)] [[PubMed](#)]
23. Wolf, E. Unified theory of coherence and polarization of random electromagnetic beams. *Phys. Lett. A* **2003**, *312*, 263–267. [[CrossRef](#)]
24. Baykal, Y. Scintillations of LED sources in oceanic turbulence. *Appl. Opt.* **2016**, *55*, 8860–8863. [[CrossRef](#)] [[PubMed](#)]
25. Liu, A.; Yuan, Y.; Yin, H. Optimization of LED Array Spatial Coverage Characteristics in Underwater Wireless Optical Communication. *J. Mar. Sci. Eng.* **2023**, *11*, 253. [[CrossRef](#)]
26. Paul, P.; Rainer, R.; Richard, K. Partially coherent light-emitting diode illumination for video-rate in-line holographic microscopy. *Appl. Opt.* **2012**, *51*, 2333–2340.
27. Zhang, Y.; Guo, H.; Qiu, X.; Lu, X.; Ren, X.; Chen, L. LED-based chromatic and white-light vortices of fractional topological charges. *Opt. Commun.* **2020**, *10*, 126732. [[CrossRef](#)]
28. Röhrich, R.; Koenderink, A.F.; Witte, S. Spatial coherence control and analysis via micromirror-based mixed-state ptychography. *New J. Phys.* **2021**, *23*, 053016. [[CrossRef](#)]
29. Gori, F.; Santarsiero, M.; Borghi, R. Intensity-based modal analysis of partially coherent beams with Hermite-Gaussian modes. *Opt. Lett.* **1998**, *23*, 989–991. [[CrossRef](#)]
30. Thorpe, S.A. *An Introduction to Ocean Turbulence*; Cambridge University Press: Cambridge, UK, 2007.

**Disclaimer/Publisher’s Note:** The statements, opinions and data contained in all publications are solely those of the individual author(s) and contributor(s) and not of MDPI and/or the editor(s). MDPI and/or the editor(s) disclaim responsibility for any injury to people or property resulting from any ideas, methods, instructions or products referred to in the content.